Proofs to:
Professor Martin Schroder,
School of Chemistry,
University of Nottingham,
Nottingham NG7 2RD.

Submission to: *Chemistry Eur. J.*

Analysis of High and Selective Uptake of CO_2 in an Oxamide-containing $\{Cu_2(OOCR)_4\}$ Based Metal Organic Framework

Nada H. Alsmail, Mikhail Suyetin, Yong Yan, Rafel Cabot, Cristina P. Krap, Jian Lü, Timothy L. Easun, Elena Bichoutskaia, William Lewis, Alexander J. Blake and Martin Schröder*

School of Chemistry, University of Nottingham, Nottingham NG7 2RD, UK.

Keywords: metal-organic framework, CO_2, methane, copper, isophthalate, carboxylic acid, amide

Abstract

The porous framework $[Cu_2(H_2O)_2L].4H_2O.2DMA$ (H_4L = oxalylbis(azanediyl)diisophthalic acid; DMA = *N,N*-dimethylacetamide), denoted NOTT-125, is formed by connection of $\{Cu_2(RCOO)_4\}$ paddlewheels with the isophthalate linkers in L^{4-}. A single crystal structure determination reveals that NOTT-125 crystallises in monoclinic cell with *a* = 27.9161(6) Å, *b* = 18.6627(4) Å and *c* = 32.3643(8) Å, space group *P*2 *(1)/c*. The structure of this material shows **fof** topology, which can be viewed as the packing of two types of cages (Cage A and Cage B) in 3-dimensional space. Cage A is constructed by twelve $\{Cu_2(OOCR)_4\}$ paddlewheels and six linkers to form an ellipsoid-shaped cavity approximately 24.0 Å along its long axis and 9.6 Å across the central diameter. Cage B consists of six $\{Cu_2(OOCR)_4\}$ units and twelve linkers with a spherical diameter of 12.7 Å taking into account the van der Waals radii of the atoms. NOTT-125 incorporates oxamide functionality within the pore walls, and this, combined with high porosity in the desolvated NOTT-125a, is responsible for excellent CO_2 uptake (40.1 wt% at 273 K and 1 bar) and selectivity for CO_2 over CH_4 or N_2. Grand canonical Monte Carlo (GCMC) simulations show excellent agreement with the experimental gas isotherm data, and a computational study into the specific interactions and binding energies of both CO_2 and CH_4 with the linkers in NOTT-125 reveals a set of strong interactions between CO_2 and the oxamide motif, which are not possible with a single amide.

Introduction

Metal-organic frameworks (MOFs) show great promise for applications in gas storage and separation because these crystalline, porous materials can demonstrate exceptionally high internal surface areas and tunable functional pore environments.[1] Notably, CO_2 storage in MOFs[2] compares extremely favourably with other classes of porous materials such as zeolites, activated carbon and silica.[3] Great efforts have been focused on enhancing the binding affinity and selectivity of MOFs towards CO_2, and several strategies have been reported to enhance gas storage.[4] The shape, size and chemical environment of the pores within a MOF play significant roles in gas storage capacity, specificity and separations.[1d,5] The physical characteristics of pore volume and surface area have been shown to correlate strongly with the high pressure (>20 bar) CO_2 uptake in MOFs, with physisorption dominating, while the strength of gas-framework interactions correlates strongly with the low pressure (<1 bar) CO_2 uptake of a framework.[6] The primary approaches to controlling the chemical characteristics of the pores and hence the strength of the gas-framework interaction are *via* modification of the ligands either by incorporating functional groups prior to the formation of MOFs or by post-synthetic modification in which functional groups such as -NH_2, -OH or -CHO moieties are generated within the frameworks.[3c,6-10] Nitrogen-containing groups or open metal sites accessible within the pores can improve CO_2 affinity via dipole-quadrupole interactions with the CO_2 molecules.[11-14] We recently described the material NOTT-122 incorporating triazole groups which displays a high adsorption capacity for CO_2 and used a computational approach to investigate the specific interactions between CO_2 and the framework linker heteroatoms.[15] Similarly, Zaworotko *et al*. have reported MOFs[16] containing amide functional groups in the linkers, whereby linking of three isophthalates generated polyhedral structures that exhibit a strong binding affinity to CO_2.[16-18]

Our general approach has been based on the use highly symmetric polydentate carboxylate ligands to construct porous coordination polymers which demonstrate excellent gas uptake and selectivity.[19-21] We describe herein the synthesis and gas uptake properties of NOTT-125, an amide-containing MOF primarily distinguished by the '*double amide*' [-NHC(O)C(O)NH-] oxamide motif within the bridging ligand L^{4-} (H_4L = oxalylbis(azanediyl)diisophthalic acid) whereby two back-to-back amides comprise the bridge between two isophthalate groups. This linker connects $\{Cu_2(OOCR)_4\}$ paddlewheels to form a MOF of **fof** topology [Fig. 1] in which the oxamide is incorporated and placed within the pore walls. NOTT-125 exhibits a high surface area and excellent CO_2 uptake (40.1% at 1 bar, 273 K). To the best of our knowledge NOTT-125 displays the third highest reported CO_2 uptake in a MOF [Table 1] and shows significant selectivity for CO_2 *vs* both N_2 and CH_4. Importantly, grand canonical Monte Carlo (GCMC) simulations of the isotherms show excellent agreement with the experimental data, and a computational study into the specific interactions and binding energies of both CO_2 and CH_4 with the linkers reveals a set of strong interactions between CO_2 and the oxamide motif which are not possible with only a single amide. This is the first time that we are aware of that the oxamide motif has been employed within a MOF design.

Results and Discussion

H_4L was synthesised in high yield by reaction of oxalyl chloride and 5-aminoisophthalic acid in tetrahydrofuran (THF) [Scheme 1]. The solvothermal reaction of H_4L and $Cu(NO_3)_2.3H_2O$ in *N*,*N*-dimethylacetamide (DMA):water (6:1) under acidic (HBF_4) conditions yielded blue crystals of $[Cu_2(H_2O)_2L].4H_2O.2DMA$ in 70% yield. We find that DMA is a better solvent than DMF in this reaction and leads to the formation of more crystalline and porous products. The as-synthesised material is insoluble in common organic

solvents and was characterised by single crystal diffraction, powder X-ray diffraction, elemental analysis and thermogravimetric analysis. A single crystal structure determination reveals that NOTT-125 crystallises in monoclinic cell with a = 27.9161(6) Å, b = 18.6627(4) Å and c = 32.3643(8) Å, space group $P2\ (1)/c$. The three-dimensional porous framework hosts DMA and H_2O solvent molecules. Two Cu(II) cations are bridged by four carboxylate groups, distributed around the Cu-Cu axis, to form a $\{Cu_2(OOCR)_4\}$ paddle-wheel node with structure extended by the bridging L^{4-} linkers to form a porous 3-D structure (Fig. S2). The overall structure of NOTT-125 has **fof** topology[22] which can be viewed as the packing of two types of cages (Cage A and Cage B) in 3-dimensional space [Fig. 1]. Cage A is constructed by twelve $\{Cu_2(OOCR)_4\}$ paddlewheels and six linkers to form an ellipsoid-shaped cavity approximately 24.0 Å along its long axis and 9.6 Å across the central diameter. Cage B consists of six $\{Cu_2(OOCR)_4\}$ units and twelve linkers with a spherical diameter of 12.7 Å taking into account the van der Waals radii of the atoms. It is worth noting that the structure is densely decorated with amide functionalities that are directly exposed in both cages. There are two types of pore window between cages A and B. The smaller window is an equilateral triangle whose vertices are occupied by $\{Cu_2(COO)_4\}$ paddlewheels with a distance of 9.3 Å between their centroids. The larger window takes the shape of an isosceles triangle (13.9 × 13.9 × 9.3 Å) constructed by two linkers and one isophthalate unit.

The total accessible volume of NOTT-125 after removal of the guest and coordinated water molecules is estimated to be 71% using the PLATON/VOID routine[23] and the calculated density of the desolvated framework is 0.672 g/cm^3. NOTT-125 shows thermal stability up to 280 ^oC by thermogravimetric analysis (TGA) [Fig. S3], and the phase purity of the bulk sample was confirmed by powder X-ray diffraction (PXRD) [Fig. S4]. The fully desolvated framework NOTT-125a was prepared by soaking the sample in acetone for five days followed by heating at 100 ^oC and 10^{-10} bar for 1 day. PXRD analysis after desolvation

indicates that the framework structure of NOTT-125a retains crystallinity and remains intact on activation [Fig. S4]**.** All subsequent analyses described below were performed on the activated NOTT-125a.

The permanent porosity of activated NOTT-125a was confirmed by gas adsorption measurements. The N_2 sorption isotherm for NOTT-125a at 77 K exhibits reversible type-I adsorption behaviour characteristic of a microporous material [Fig. S5]. The Brunauer-Emmett-Teller (BET) surface area was measured as 2447 $m^2 g^{-1}$ [Fig. S6] based upon the N_2 sorption isotherm, and the calculated total pore volume of NOTT-125a is 1.1 $cm^3 g^{-1}$. The pore size distribution (PSD) was calculated according to the N_2 isotherm using non-local density functional theory (NLDFT) implementing a hybrid kernel based on a zeolite–silica model containing cylindrical pores. The PSD was found to lie in the range 10−13 Å [Fig. S7], consistent with the single crystal structure determination.

The gravimetric CH_4 sorption isotherms for NOTT-125a were recorded up to 1 bar at 273 and 298 K, both isotherms showing type-I behaviour with good reversibility and a moderate total uptake of CH_4 of 2.10 wt% (1.31 mmol g^{-1}) and 1.34 wt% (0.837 mmol g^{-1}), respectively. By comparison, the related amide-containing PCN-124 framework described by Zhou *et al*. shows CH_4 uptake of 2.33 wt% at 273 K.[24] At 20 bar NOTT-125 shows a CH_4 uptake of 20.4 wt % [192 cm^3/cm^3(STP), STP: standard temperature and pressure] at 273 K and 15.1 wt % [142.1 cm^3/cm^3] at 298 K [Fig. 4]. The isosteric heat of CH_4 adsorption was found by virial analysis to be 14.5 kJ mol^{-1} at zero surface coverage [Fig. S10].

Combined with the large pore volume, the oxamide groups in the pore walls were expected to enhance uptake of CO_2 in the framework and indeed this is evident in the low pressure (up to 1 bar) isotherms recorded at 273 and 298 K. Both isotherms are completely reversible and show no hysteresis. At 273 K, the total uptake reaches 40.1 wt% (9.09 mmol g^{-1}, 203.7 $cm^3 g^{-1}$) [Fig. 2]. At 298 K the total uptake is 18.19 wt % (4.13 $mmolg^{-1}$, 92.59 $cm^3 g^{-}$

^{1}) [Fig. 2]. The total CO_2 uptake is approaching the highest reported values for MOFs such as Cu-TDPAT[25] (44.5 wt%, 273 K, 1 bar) and Cu-TPBTM[16a] (42.6 wt%, 273 K, 1 bar) and a comparison with a range of relevant MOFs is presented in Table 1. Significantly, in comparison with the related amide-functionalised MOF Cu-NJU-Bai3,[26] NOTT-125a shows higher CO_2 uptake at 1 bar (NJU-Bai3: 27.32 wt%, 6.21 mmol g^{-1}, 273 K) and also higher uptake under the same conditions than the amide functionalised MOF PCN-124[24] (28.6 wt%, 6.5 mmol g^{-1}, 273 K). NOTT-125a also shows a high CO_2 uptake of 21.2 mmol g^{-1} at 298 K and 20 bar [Fig. 3].

The excellent uptake of CO_2 observed in the low pressure isotherms is consistent with the presence of specific CO_2-amide interactions. There are several potential interactions that can be proposed including dipole-quadrupole interactions of the type described above[11-14] and hydrogen-bond formation between the amide NH and the oxygens of CO_2.[16] To better understand these observations, the isosteric heat (Q_{st}) of adsorption of CO_2 was calculated by fitting the CO_2 sorption isotherms at 273 K and 298 K to a virial-type equation. The isosteric heat is estimated to be 25.35 kJ mol^{-1} at zero surface coverage.

The marked difference in CH_4 and CO_2 adsorption isotherms encouraged us to examine the capability of NOTT-125a for selective capture of CO_2 *vs* N_2 and CO_2 *vs* CH_4. To evaluate the selective CO_2 capture in NOTT-125a, CH_4 and N_2 sorption isotherms were measured at 273 and 298 K [Fig. 2b] up to 1 bar. By determining the ratios of the Henry's law constants from single component isotherms,[27] the CO_2/N_2 adsorption selectivity factors for NOTT-125a are 20.7:1 at 273 K and 16:1 at 298 K, further suggesting that the polar amide functionalities have a positive effect on CO_2 adsorption. Furthermore, NOTT-125a also shows respectable CO_2/CH_4 selectivity of 9.2:1 at 273 K and 4.8:1 at 298 K.

Gravimetric H_2 sorption measurements performed on NOTT-125a at 77 K and 87 K up to 1 bar show completely reversible isotherms with an absence of hysteresis and moderate

H_2 storage capacity of 2.30 % and 1.48 % respectively [Fig. 5]. The isosteric heats of adsorption (Q_{st}) for H_2 were found to be 5.1 kJ mol^{-1} at zero surface coverage.

Grand canonical Monte Carlo (GCMC) calculations were performed to simulate the adsorption of both CO_2 and CH_4 in NOTT-125a. Figures 3 and 4 show simulated isotherms for CO_2 and CH_4 uptake in NOTT-125a, and these are in excellent agreement with the experimentally measured isotherms. To understand further the relevant adsorption mechanisms of the CH_4 and CO_2 molecules to the linkers of NOTT-125a at a molecular level, second order Møller-Plesset perturbation theory (MP2) as implemented in the Q-Chem quantum chemistry package[28] was employed. We analysed the strength of two preferential adsorption sites in the linker: one formed by two amide -CONH- groups (highlighted blue in Fig. 6) and the other being the phenyl ring (highlighted red in Fig. 6). We calculated the binding energies (BE) between the guest molecule and the linker as well as their relative positions corresponding to the strongest binding. For the interactions of CH_4 and CO_2 with the oxamide part of the linker, the calculations were performed in two-stages in both cases. For CH_4, the geometry optimization was carried out using DFT calculations at the B3LYP/ 6-31G** level of theory and the binding energies were subsequently calculated at the higher B3LYP /6-311++G** level with BE = E_{opt}(complex) - E_{opt}(linker) - E_{opt}(guest molecule). For CO_2, the geometry optimization was first performed at the MP2/cc-pvdz level of theory and the binding energies were subsequently calculated at the higher MP2/cc-pvqz level. Binding energies were corrected for the basis set superposition error (BSSE), and the stable configuration identified for the CH_4 molecule and linker is shown in Fig. 7. The distance between H(CH_4) and O(amide) is less than the sum of their van der Waals radii, with the binding energy E = -5.57 kJ/mol characterized by a hydrogen bond-like interaction, C(CH_4)-H(CH_4)···O(amide), with a C-H···O angle of 178.85^o.

We performed an extensive search for CO_2 binding sites and several configurations showing the strongest binding are summarised in Tables 2 and 3. The strongest binding of CO_2 to the linker was found to be in complexes A and B in which the guest CO_2 molecule interacts with the linker in a side on fashion and having binding energies of -19.7 kJ/mol and -16.2 kJ/mol, respectively. In complex A the interaction is dominated by a strong hydrogen bond (2.30 Å) formed between the electronegative oxygen of CO_2 and hydrogen of the amide group. This interaction is further enhanced by both the electrostatic attraction between the carbon of CO_2 and the electronegative oxygen of the linker, and a weak C-O···H-C(aromatic) interaction which can be regarded as as a weak hydrogen bond.[29] All these interactions have a significant cooperative effect on the overall binding of CO_2 to this polyamide core. Complex B corresponds to an in-plane T-shape orientation of CO_2 and the C-O bond of one of the amide groups of the linker. The electrostatic interaction between carbon of CO_2 and oxygen in the linker is somewhat stronger in this configuration compared to complex A. Complex C (BE = -14.92 kJ/mol) is stabilised by two hydrogen bonds N-H···$O_1(CO_2)$ and N-H···$O_2(CO_2)$, thus having one donor and two acceptors. The N-H···$O_1(CO_2)$ angle of 129.69^o is fairly close to the ideal value of 120^o, which may explain the relatively high value of the binding energy. Similarly, a hydrogen bond-like interaction C-H···$O_1(CO_2)$ (the corresponding angle is 125.42^o) and an electrostatic interaction between carbon of CO_2 and oxygen in the linker are also present.

Complexes D-G correspond to the CO_2 molecule being located above the oxamide group. A relatively strong binding has been found when the CO_2 molecule is located in a 'bay' formed by a phenyl ring and the amide group (complex D, BE = -13.04 kJ/mol). Complex E (BE = -12.67 kJ/mol) highlights the importance of coulombic interactions between carbon dioxide and the linker, in which the carbon of CO_2 is located directly above an oxygen of the linker, and an oxygen of CO_2 is found above the carbon of the linker.

Complex F (BE = -10.25 kJ/mol) shows CO_2 positioned above the N-C bond, between the phenyl ring and an amide group. The least favourable binding site is found to be dimer G (BE = -7.61 kJ/mol) where the CO_2 molecule is located approximately mid-way between the carbons of the C-C bond between the two amide groups, but even this binding energy is stronger than that found for methane binding described above.

Finally, we compared the interactions of the CO_2 molecule with the oxamide part of the linker against those of CO_2 and solely the phenyl group (blue in Fig. 6), which has been replaced by a benzene ring. As this complex is somewhat smaller, more accurate calculations were undertaken in which both geometry optimization and the BSSE-corrected binding energies were obtained directly at the MP2/cc-pvqz level of theory. Five stable configurations of the CO_2 molecule and benzene ring are presented in Table 4. The strongest interaction corresponds to the cases where the carbon atom of CO_2 is located directly above the middle of the benzene ring (complexes H and I). In the case of complex H (BE = -11.13 kJ/mol) the oxygen atoms of CO_2 are above the middle of two C-C bonds of the benzene ring, and the distances between the oxygen atoms of CO_2 and the nearest carbon atoms in the benzene ring are in the range of 3.34 Å to 3.39 Å. In complex I (BE = -10.54 kJ/mol), the oxygen atoms of CO_2 are above the carbon atoms of the benzene ring and the corresponding separation is slightly greater, being in the range of 3.44 Å to 3.52 Å. The predicted values of the binding energies are in excellent agreement with previous calculations.[30] The remaining three configurations (complexes J-L) are far less stable (BE in the range of -2 kJ/mol to -4 kJ/mol) and these correspond to the orientations in which where CO_2 interacts side-on with the benzene ring.

Our calculations confirm that the oxamide part of the linker provides a variety of strong binding sites for CO_2 molecules with the values for the binding energy being significantly greater than those identified between CO_2 and the phenyl group, thus offering a

clear preferential binding region in NOTT-125a. These binding modes are clearly not accessible in frameworks containing only single amides in their linkers. Additionally, in contrast to the CO_2−oxamide interactions, the binding identified between NOTT-125a and CH_4 is dependent on the presence of only one of the amide groups of the linker. The selectivity of NOTT-125a for CO_2 over CH_4, therefore, seems likely to be strongly influenced by the presence of this previously under-investigated oxamide motif.

Conclusions

In conclusion, we have successfully constructed a new highly porous **fof** type Cu(II) paddlewheel porous material, the first reported example of a MOF containing the oxamide functional group. Two types of cage exist within NOTT-125, both of which are bounded by the oxamide functionality. The large pore volume and functionalised pores are responsible for NOTT-125a exhibiting high CO_2 gas storage capacity and selectivity of CO_2 uptake over N_2 and CH_4. GCMC simulations of the gas uptake isotherms show excellent agreement with the experimental data and our computational studies of the binding modes of CH_4 and CO_2 in NOTT-125a has identified a variety of strong binding sites for CO_2, which are only possible with the oxamide functionality.

Experimental

Commercially available reagents were used as received without further purification. Elemental analyses (C, H, and N) were performed on a CE-440 elemental analyzer at the University of Nottingham. IR spectra were recorded in the range of 550−4000 cm^{-1} on a Nicolet i5 FT-IR spectrophotometer using the attenuated total reflectance (ATR) mode. ^1H NMR spectra were recorded on a Bruker DPX-300 spectrometer. Thermal gravimetric analyses (TGA) were performed under a flow of nitrogen (20 mL/min) with a heating rate of

1 °C/min using a TA SDT-600 thermogravimetric analyzer. X-ray Powder Diffraction (PXRD) measurements were carried out at room temperature on a PANalytical X'Pert PRO diffractometer using Cu-*Kα* radiation (λ = 1.5418 Å) at 40 kV, 40 mA, at a scan speed of 0.02°/s and a step size of 0.005° in 2θ.

N_2, H_2 and CO_2 Isotherms. N_2, H_2 and CO_2 isotherms were determined using an IGA gravimetric adsorption apparatus (Hiden) at the University of Nottingham in a clean ultra high vacuum system with a diaphragm and turbo pumping system. Before measurements, about 120 mg of solvent-exchanged sample was loaded into the sample basket within the adsorption instrument and then degassed under dynamic vacuum at 100 °C for 16 h to obtain the fully desolvated samples.

Synthesis of H_4L: A solution of 5-aminoisophthalic acid (6.53 g, 34.2 mmol) in anhydrous THF (50 mL) was cooled at 0˚C. A solution of oxalyl chloride (1.0 mL, 11.4 mmol) in anhydrous THF (100 mL) was then added dropwise to the reaction mixture over a period of 1 h. and a precipitate formed almost immediately. Triethylamine (1.0 mL, 7.2 mmol) was slowly added after 1 h. and the mixture was stirred overnight (~12 h) at room temperature. The volume of solvent was partially reduced in the rotary evaporator and then 200 mL of 2M HCl were added to the mixture. The precipitate was isolated by filtration and washed extensively with water, recrystallised from methanol, filtered, washed with methanol and diethyl ether, and dried under vacuum to afford a white powder (2.47 g, 58 % yield). ^{1}H NMR (300 MHz, DMSO-d_6): δ (ppm) = 13.08 (s, 4H, COOH), 11.26 (s, 2H, NH), 8.72 (d, J = 1.2 Hz, 4H, Ar-H), 8.26 (t, J = 1.2 Hz , 2H, Ar-H); ^{13}C NMR (75 MHz, DMSO-d_6): δ (ppm) = 166.81, 159.24, 138.80, 132.30, 126.43, 125.68 ; ATR FT-IR: (cm^{-1}) = 3227 (m), 2158 (w), 1974 (w), 1716(s), 1681(s), 1653(s), 1558 (m), 1540 (s), 1456 (m), 1387 (s), 1275 (s), 1301(m), 1185 (w), 952 (m), 841(m), 758 (s), 728 (s), 670 (m); HRMS (EI-): *m/z* =

439.0403 $(M+Na)^+$, 434.0838 $(M+H_4N)^+$, 415.0401 $(M-H)^-$. Anal. Calcd (Found) for $C_{18}H_{12}N_2O_{10}$: C, 51.93 (51.47); H, 2.98 (3.05); N, 6.73 (6.56).

Synthesis of NOTT-125, $[Cu_2(C_{18}H_{12}O_{10}N_2](H_2O)_2]\bullet 2DMA\bullet 4H_2O$. H_4L (0.03 g, 0.081 mmol) and $Cu(NO_3)_2\bullet 3H_2O$ (0.06 g, 0.516 mmol) were added to a DMA:H_2O solvent (9:2, 5.5 ml). HBF_4 (50% in H_2O, 0.2 mL) was added and the solution thoroughly mixed. The solution was heated without stirring at 70 ^oC using an oil bath for 48 h and a large amount of microcrystalline product precipitated. The blue crystalline product was separated by filtration, washed with warm DMA and dried briefly in air. Yield: 0.15 g (60%). Anal. Calcd (Found) for $C_{26}H_{38}Cu_2N_4O_{18}$: C, 38.00 (39.10); H, 4.60 (4.82); N, 6.82 (6.85).

Crystallographic data have been deposited with the Cambridge Crystallographic Data Centre as supplementary publications CCDC 965874 for NOTT-125. Supporting information includes additional views of the crystal structures, TGA and PSD analysis, PXRD, technical details for gas adsorption experiments and gas isotherms.

Acknowledgements

We thank the EPSRC and the University of Nottingham for support and funding. MS gratefully acknowledges receipt of an ERC Advanced Grant, and EB for an ERC Starter Grant. NHA thanks the Royal Commission for Jubail and Yanbu, Jubail University College, Kingdom of Saudi Arabia for a PhD Fellowship, CPK thanks Conacyt, Mexico for funding, and LU thanks the Royal Society for a Sino-British Fellowship.

References:

[1] (a) H. Furukawa, N. Ko, Y. B. Go, N. Aratani, S. B. Choi, E. Choi, A.Ö. Yazaydin, R. Q. Snurr, M. O'Keeffe, J. Kim, O. M. Yaghi, *Science* **2010,** *329*, 424-428; (b) O. K. Farha, A. Ö. Yazaydin, I. Eryazici, C. D. Malliakas, B. G. Hauser, M. G. Kanatzidis, S. T. Nguyen, R. Q. Snurr, J. T. Hupp, *Nat. Chem.* **2010**, *11*, 944-948; (c) J.-R. Li, J. Sculley, H.-C. Zhou, *Chem. Rev*. **2012**, *112*, 869-932; (d) K. Koh, A. G. Wong-Foy, A. J. Matzger, *J. Am. Chem. Soc.* **2009**, *131*, 4184-4185; (e) S. Yang, X. Lin, A. J. Blake, G. S. Walker, P. Hubberstey, N. R. Champness, M. Schröder, *Nat. Chem.* **2009**, *1*, 487-493; (f) X. Lin, J. Jia, X. B. Zhao, K. M. Thomas, A. J. Blake, N. R. Champness, P. Hubberstey, M. Schröder, *Angew. Chem., Int. Ed.* **2006**, *45*, 7358-7364; (g) X. Lin, J. Jia, P. Hubberstey, M. Schröder, N. R. Champness, *CrystEngComm* **2007**, *9*, 438-448.

[2] (a) J. Liu, P. K. Thallapally, B. P. McGrail, D. R. Brown, J. Liu, *Chem. Soc. Rev*. **2012**, *41*, 2308−2322; (b) D. M. D'Alessandro, B. Smit, J. R. Long, *Angew. Chem., Int. Ed.* **2010**, *49*, 6058-6082; (c) A. R. Millward, O. M. Yaghi, *J. Am. Chem. Soc.* **2005**, *127*, 17998-17999.

[3**]** (a) Z. Zhang, Y. Zhao, Q. Gong, Z. Li, J. Li, *ChemComm.* **201**3, *49*, 653-661; (b) J-R. Li, Y. Ma, M. C. McCarthy, J. Sculley, J. Yu, H-K. Jeong, B.Balbuena, H-C. Zhou, *Coord. Chem. Rev.* **2011**, *255*, 1791-1823; (c) K. Sumida, D. L. Rogow, J. A. Mason, T. M. McDonald, E. D. Bloch, Z. R. Herm, T.-H. Bae, J. R. Long, *Chem. Rev.* **2012**, *112*, 724-781

[4] (a) W. Yang, A. J. Davies, X. Lin, M. Suyetin, R. Matsuda, A. J. Blake, C. Wilson, W. Lewis, J. E. Parker, C. C. Tang, M. W. George, P. Hubberstey, S. Kitagawa, H. Sakamoto, E. Bichoutskaia, N. R. Champness, S. Yang, M. Schröder, *Chem. Sci.* **2012**, *3*, 2993-2999; (b) S. Yang, X. Lin, W. Lewis, M. Suyetin, E. Bichoutskaia, J. Parker, C. C. Tang, D. R. Allan, P. J. Rizkallah, P. Hubberstey, N. R. Champness, K. M. Thomas, A. J. Blake, M. Schröder, *Nat. Mater.* **2012**, *11*, 710-716; (c) S. Yang, J. Sun, A. J. Ramirez-Cuesta, S. K. Callear, W. I. F.

David, D. Anderson, R. Newby, A. J. Blake, J. E. Parker, C. C. Tang, M. Schröder, *Nat. Chem.* 2012, *4*, 887-894.

[5] (a) D. M. D'Alessandro, B. Smit, J. R. Long, Angew. *Chem. Int. Ed*. **2010**, *49*, 6058-6082; (b) A. R. Millward, O. M. Yaghi, *J. Am. Chem. Soc.* **2005**, *127*, 17998-17999; (c) L. J. Murray, M. Dincă, J. R. Long, *Chem. Soc. Rev*. **2009**, *38*, 1294-1314; (d) H. Furukawa, M. A. Miller, O. M. Yaghi, *J. Mater. Chem.* **2007**, *17*, 3197-3204.

[6] (a) X. Lin, N. R. Champness, M. Schröder, *Top. Curr. Chem.* **2010**, *293*, 35-76; (b) X. Lin, J. Jia, P. Hubberstey, M. Schröder, N. R. Champness, *CrystEngComm* **2007**, *9*, 438-448; (c) L. J. Murray, M. Dincă, J. R. Long, *Chem. Soc. Rev*. **2009**, *38*, 1294-1314.

[7] Y. Zhao, H. Wu, T. J. Emge, Q. Gong, N. Nijem, Y. J. Chabal, L. Kong, D. C. Langreth, H. Liu, H. Zeng, J. Li, *Chem. Eur. J.* **2011**, *17*, 5101-5109.

[8] X. Si, C. Jiao, F. Li, J. Zhang, S. Wang, S.Liu, Z. Li, L. Sun, F. Xu, Z.Gabelica, C.Schick, *Energy Environ. Sci*. **2011**, *4*, 4522-4527.

[9] C. Zlotea, D. Phanon, M. Mazaj, D. Heurtaux, V. Guillerm, C. Serre, P. Horcajada, T.Devic, E.Magnier, F. Cuevas, G. Férey, P. L. Llewellyn, M. Latroche, *Dalton Trans*. **2011**, *40*, 4879-4881.

[10] A. Demessence, D. M. D'Alessandro, M. L. Foo, J. R. Long, *J. Am. Chem. Soc*. **2009**, *131*, 8784-8786.

[11] (a) R. Vaidhyanathan, S. S. Iremonger, K. W. Dawson, G. K. H. Shimizu, *ChemComm.* **2009**, 5230-5232; (b) S. Couck, J. F. M. Denayer, G. V. Baron, T. Remy, J. Gascon, F. Kapteijn, *J. Am. Chem. Soc.* **2009**, *131*, 6326-6327.

[12] F. Debatin, A. Thomas, A. Kelling, N. Hedin, Z. Bacsik, I. Senkovska, S. Kaskel, M. Junginger, H. Müller, U. Schilde, C. Jager, A. Friedrich, H.-J. Holdt, *Angew. Chem., Int. Ed.* **2010**, *49*, 1258-1262.

[13] J. An, S. J. Geib, N. L. Rosi, *J. Am. Chem. Soc*. **2010**, *132*, 38-39.

[14] B. Arstad, H. Fjellvåg, K. Kongshaug, O. Swang, R. Blom, *Adsorption* **2008**, *14*, 755-762.

[15] Y. Yan, M. Suyetin, E. Bichoutskaia, A. J. Blake, D. R. Allan, S. A. Barnett, M. Schröder, *Chem. Sci.* **2013**, *4*, 1731-1736.

[16] (a) B. Zheng, J. Bai, J. Duan, L. Wojtas, M. J. Zaworotko, *J. Am. Chem. Soc*. **2011**, *133*, 748-751; (b) a) D. Q. Yuan, D. Zhao, D. F. Sun, H-C. Zhou, *Angew. Chem. Int. Ed.* **2010**, *49*, 5357-5361

[17] B. Chen, S. Xiang, G. Qian, *Acc. Chem. Res.* **2010**, *43*, 1115-1124.

[18] P. D. C. Dietzel, V. Besikiotis, R. Blom, *J. Mater. Chem*. **2009**, *19*, 7362-7370.

[19] M. Dincă, J. R. Long, *Angew. Chem. Int. Ed*. **2008**, *47*, 6766-6779.

[20] (a) X. Lin, I. Telepeni, A. J. Blake, A. Dailly, C. Brown, J. Simmons, M. Zoppi, G. S. Walker, K. M. Thomas, T. J. Mays, P. Hubberstey, N. R. Champness, M. Schröder, *J. Am. Chem. Soc*. **2009**, *131*, 2159-2171; (b) Y. Yan, X. Lin, S. Yang, A. J. Blake, A. Dailly, N. R. Champness, P. Hubberstey, M. Schröder, *Chem.Comm.* **2009**, 1025-1027; (c) Y. Yan, I. Telepeni, S. Yang, X. Lin, W. Kockelmann, A. Dailly, A. J. Blake, W. Lewis, G. S. Walker, D. R. Allan, S. A. Barnett, N. R. Champness, M. Schröder, *J. Am. Chem. Soc.* **2010**, *132*, 4092-4094; (d) Y. Yan, A. J. Blake, W. Lewis, S. A. Barnett, A. Dailly, N. R. Champness, M. Schröder, *Chem.–Eur. J.* **2011**, *17*, 11162-11170.

[21] Y.Yan, S. Yang, A. J. Blake, W. Lewis, E. Poirier, S. A. Barnett, N. R. Champness, M. Schröder, *ChemComm.* **2011**, *47*, 9995-9997.

[22] (a) M. O'Keeffe and O. Yaghi, *Chem. Rev*. **2012**, *112*, 675-702; (b) Z. Wang, B. Zheng, H. Liu, X. Lin, X. Yu, P. Yi, R. Yun, *Cryst. Growth Des*. **2013**, in press. DOI: 10.1021/cg401180r.

[23] A. L. Spek, PLATON, *Acta Crystallogr. Sect. D: Biol. Crystallogr.* **2009**, *65*, 148-155.

[24] J. Park, J.-R. Li, Y.-P. Chen, J. Yu, A. A. Yakovenko, Z. U. Wang, L.-B. Sun, P. B. Balbuena, H.-C. Zhou, *ChemComm.* **2012**, *48*, 9995-9997.

[25] (a) B. Li, Z. Zhang, Y. Li, K. Yao, Y. Zhu, Z. Deng, F. Yang, X. Zhou, G. Li, H. Wu, N. Nijem, Y. J. Chabal, Z. Lai, Y. Han, Z. Shi, S. Feng, J. Li , *Angew. Chem. Int. Ed*. **2012**, *51*, 1412-1415. (b) R. Luebke, J. F. Eubank, A. J. Cairns, Y.Belmabkhout, L. Wojtas, M. Eddaoudi, *ChemComm.* **2012**, *48*, 1455-1457.

[26] (a) B. Zheng, H. Liu, Z. Wang, X. Yu, P. Yi, J. Bai, *CrystEngComm* **2013**, *15*, 3517-3520; (b) B. Zheng, Z. Yang, J. Bai, Y. Li, S. Li, *ChemComm.* **2012**, *48*, 7025-7027; (c) J. Duan, Z. Yang, J. Bai, B. Zheng, Y. Li, S. Li, *ChemComm.* **2012**, *48*, 3058-3060; (d) Z. Lu, H. Xing, R. Sun, J. Bai, B. Zheng, Y. Li, *Cryst. Growth Des.* **2012**, *12*, 1081-1084.

[27] M. S. Sun, D. B. Shah, H. H. Xu, O. Talu, *J. Phys. Chem. B* **1998**, *102*, 1466-1473.

[28] A. Gupta, S. Chempath, M. J. Sanborn, L. A. Clark, R. Q. Snurr, *Mol. Simul.* **2003**, *29*, 29-46.

[29] (a) G.R. Desiraju, T. Steiner, The weak hydrogen bond: in structural chemistry and biology. Oxford: Oxford University Press, 1999; (b) G.R. Desiraju, *Acc. Chem. Res.* **1991**, *24*, 290-296; (c) S. Varughese, S. M. Drapper, *Cryst. Growth Des.* **2010**, ***10***, 2298-2305.

[30] S.S. Han, D. Kim, D. H. Jung, S. Cho, S. –H. Choi,Y. J. Jung, *J. Phys. Chem. C*. **2012**, ***116***, 20254-20261.

Figures,Tables and Schemes

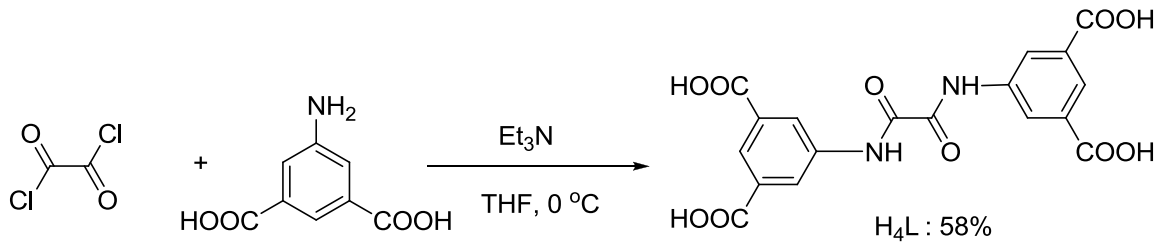

Scheme 1: Synthesis of H_4L

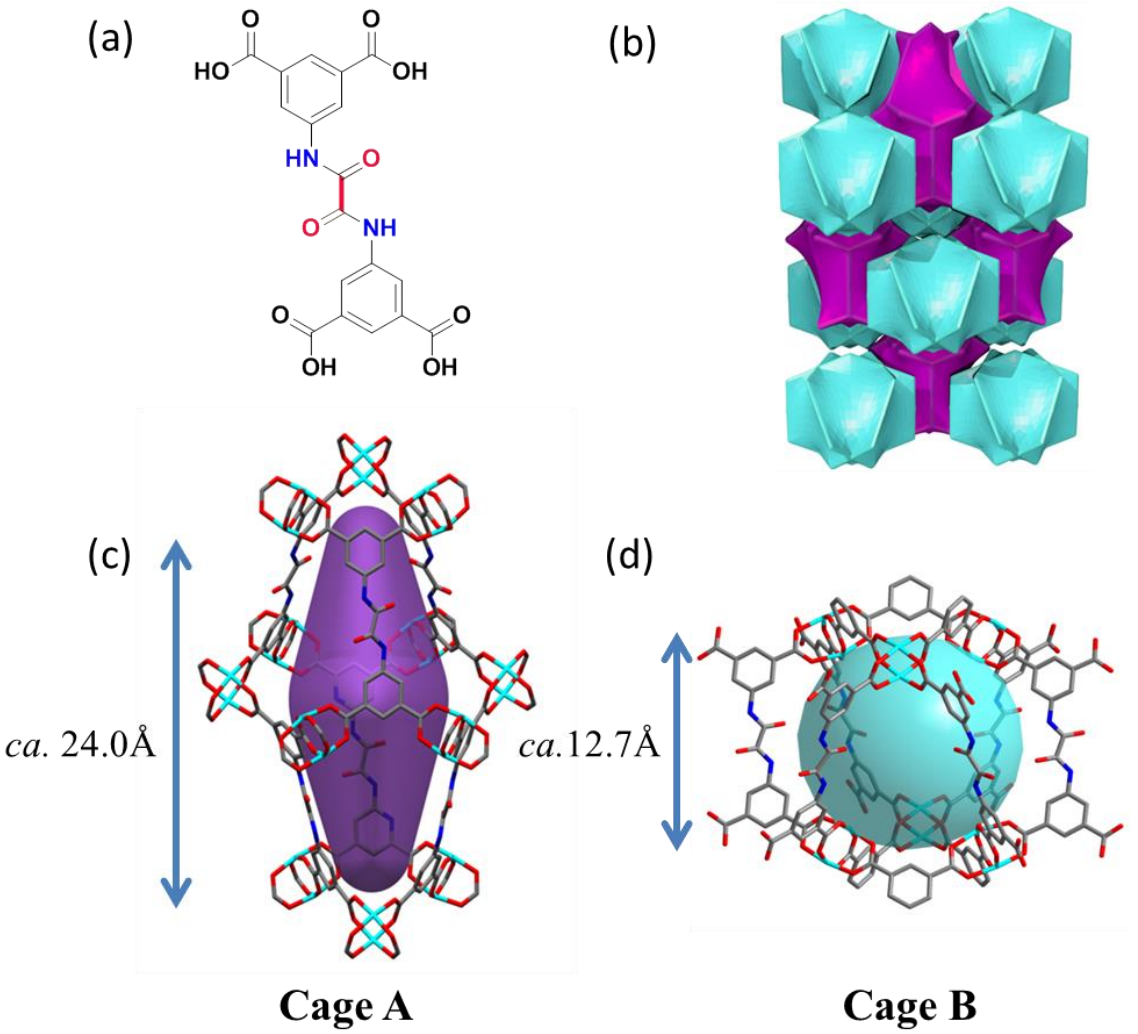

Figure 1: View of (a) chemical structure of H_4L; (b) a natural tiling of NOTT-125; (c) Cage ***A*** and (d) Cage ***B***.

Material	BET (m^2g^{-1})	Pore volume (cm^3g^{-1})	CO_2 uptake wt% at 273 K, 1 bar	CO_2 uptake wt% at 298 K, 1 bar	Q_{st} ($kJmol^{-1}$)	Reference
NJU-Bai-3	2690	1.08	27.3	10.0	36.5	26
[Cu_3(TPBTM)]	3160	1.27	42.6	23.28	26.3	16a
[Cu_3(TDPAT)	1938	0.93	44.5	25.8	42.2	25
PCN-124	1372	0.58	28.6	-	26.3	24
[Cu_3(BDPT)] HNUST-1	1400	0.57	30.7	18.26	31.2	26
NOTT-125	2471	1.1	40.0	18.19	25.4	This work
NOTT-122	3286	1.41	39.7	20.4	24.5	15
PCN-61	3350	1.37	21.4	-	22.0	16b
PCN-66	4000	1.63	22.1	-	26.2	16b
PCN-68	5109	2.13	22.1	-	21.2	16b

Table 1: Surface area, CO_2 uptake and Q_{st} values for selected MOFs.

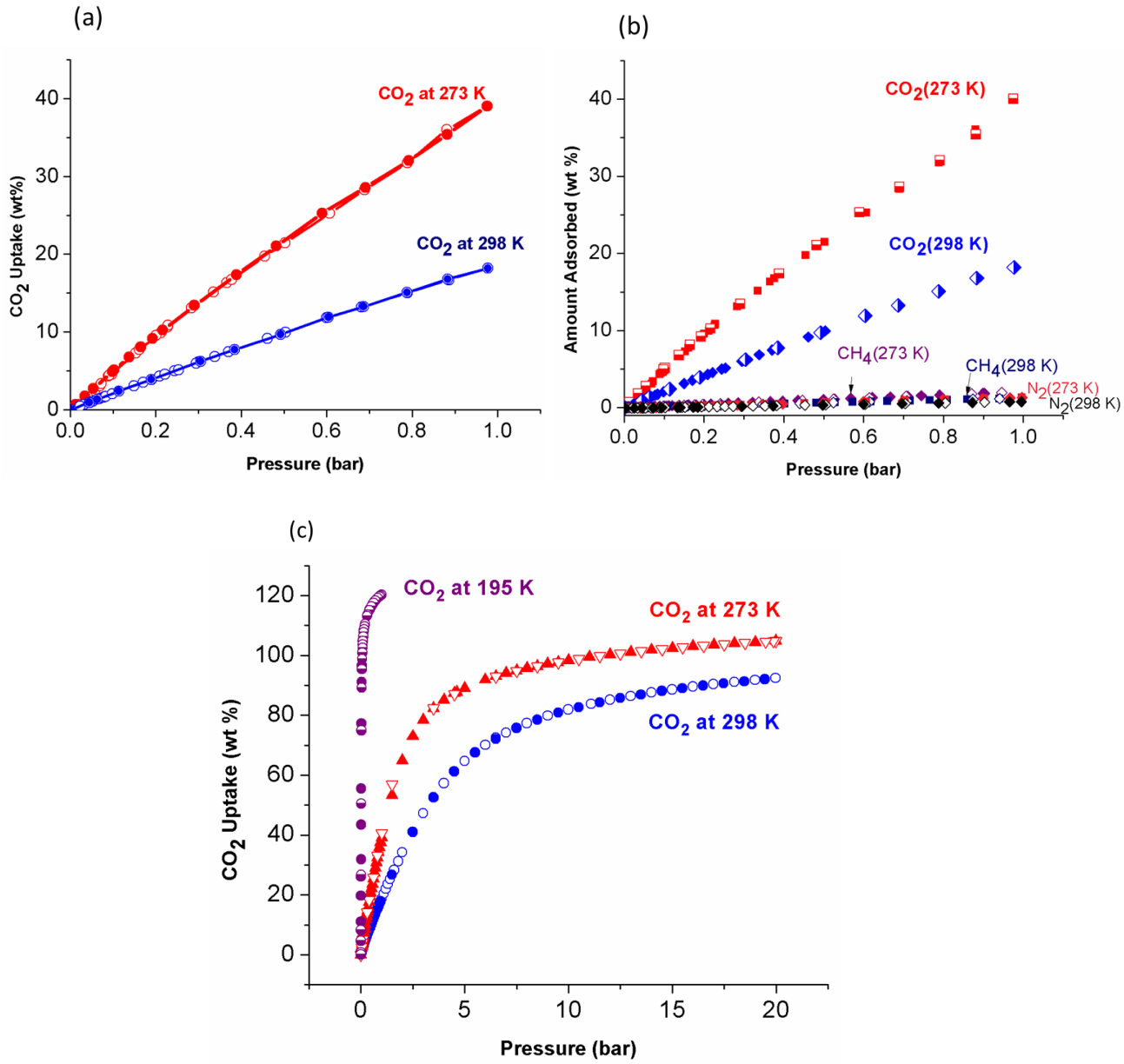

Figure 2 a) CO_2 sorption isotherms of NOTT-125a at 273 K and 298 K up to 1 bar; b) CO_2, CH_4 and N_2 sorption isotherms for NOTT-125a at 273 and 298 K up to 1 bar and c) CO_2 sorption isotherms of NOTT-125a at 195 K, 273 K and 298 K up to 20 bar.

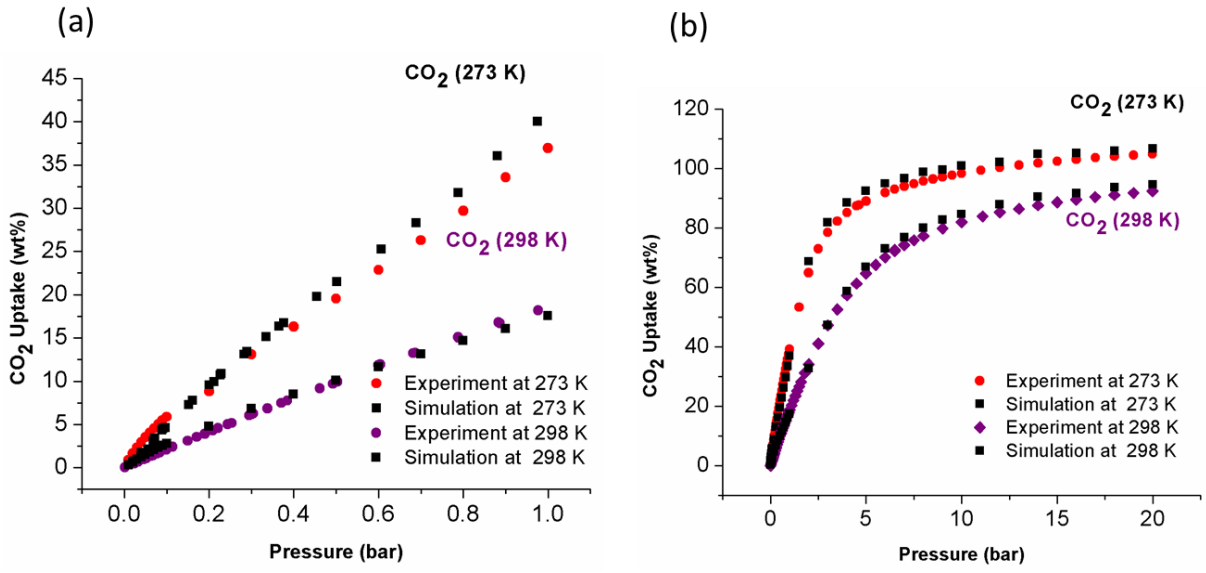

Figure 3 a) Experimental and simulated CO_2 isotherms of NOTT-125a at 273 K and 298 K in the pressure range 0-1 bar; b) Experimental and simulated CO_2 isotherms of NOTT-125a at 273 K and 298 K up to 20 bar.

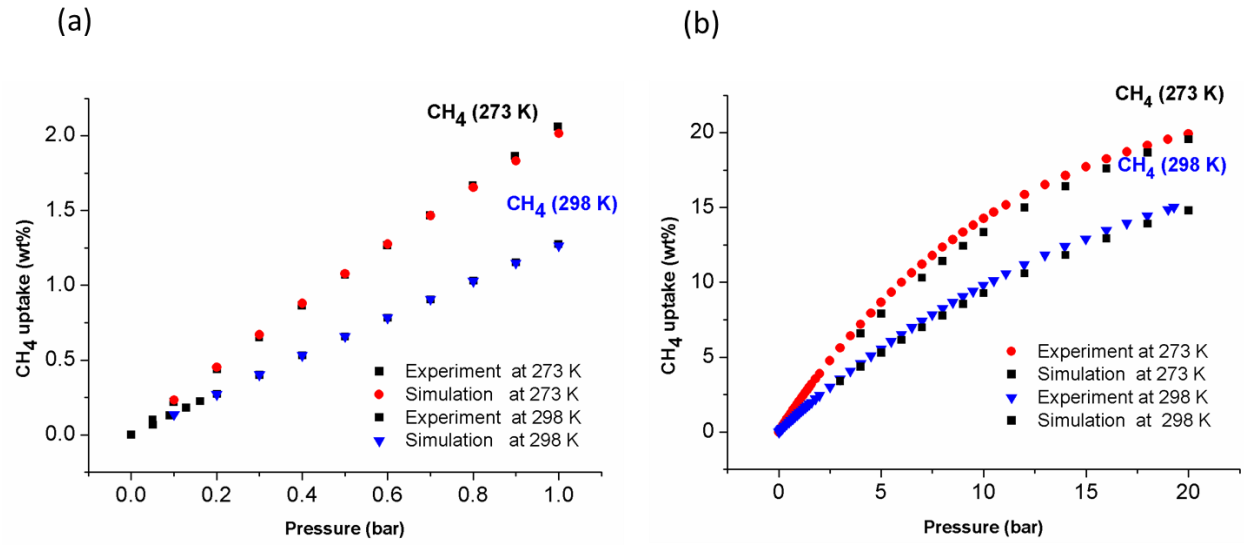

Figure 4: a) Experimental and simulated CH_4 isotherms of NOTT-125a at 273 K and 298 K in the pressure range 0- 1 bar; b) Experimental and simulated CH_4 isotherms of NOTT-125a at 273 K and 298 K up to 20 bar.

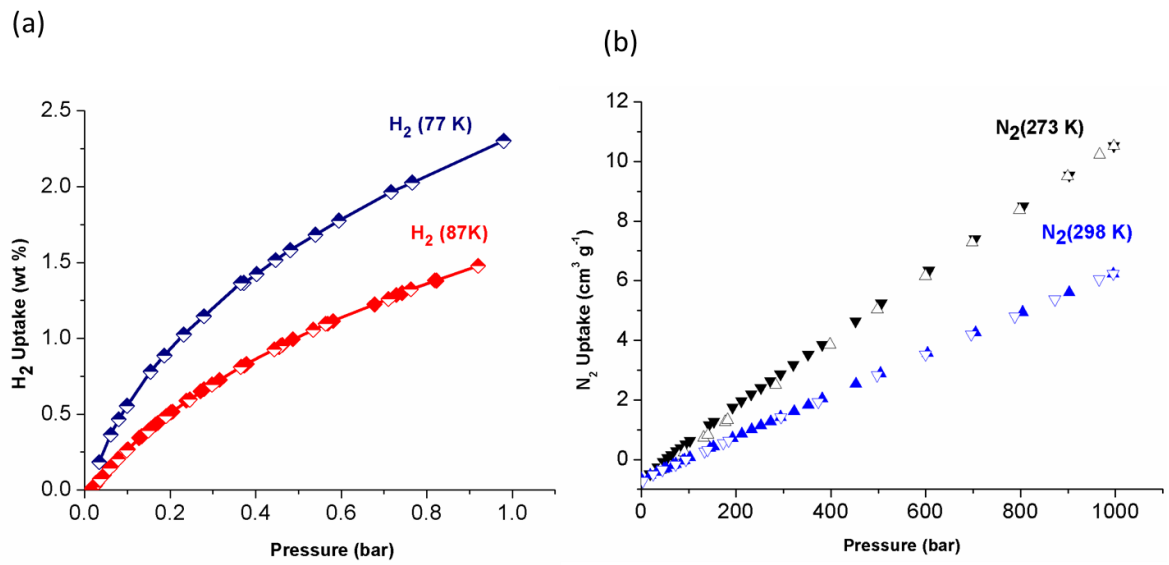

Figure 5: a) H_2 isotherms of NOTT-125a at 77 K and 87 K up to 1 bar; b) N_2 isotherms of NOTT-125a at 273 K and 298 K up to 1 bar.

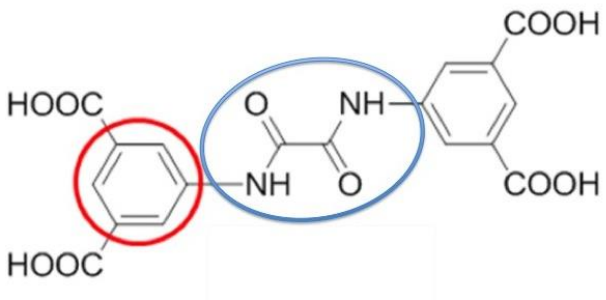

Figure 6: Two adsorption sites for CO_2 on the NOTT-125a linker examined by the calculations: the oxamide part highlighted in blue, and phenyl ring highlighted in red.

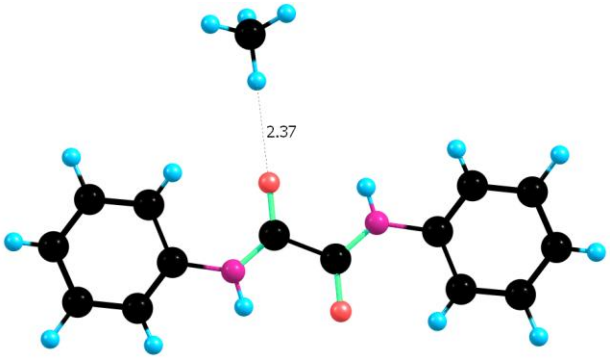

Figure 7: The optimised geometry of the $C_{14}H_{12}N_2O_2 - CH_4$ complex.

Table 2: The optimised MP2/cc-pvdz geometries and MP2/cc-pvqz binding energies of $C_{14}H_{12}N_2O_2$ - CO_2 complexes.

	Optimised Geometry	Binding Energy, kJ/mol
A	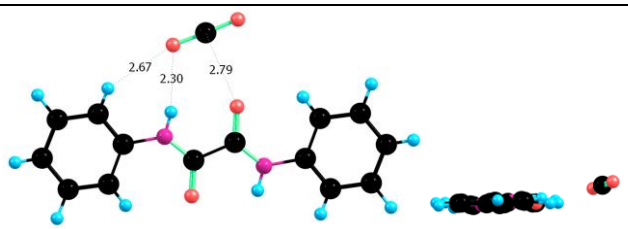	-19.66
B	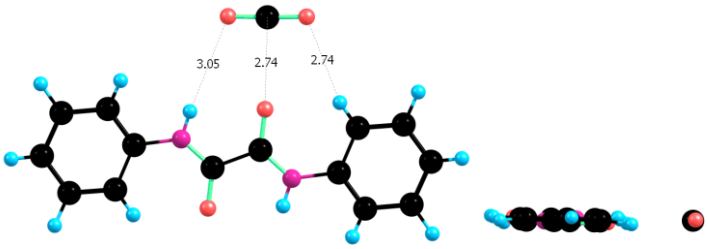	-16.17
C	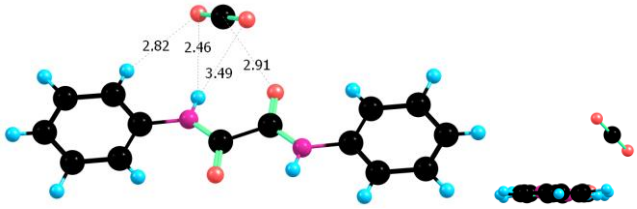	-14.92
D	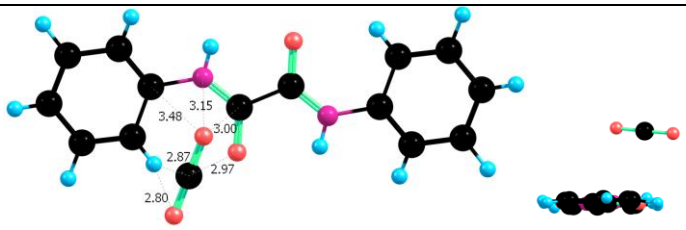	-13.04
E	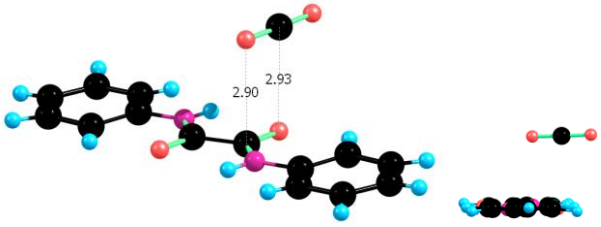	-12.67
F	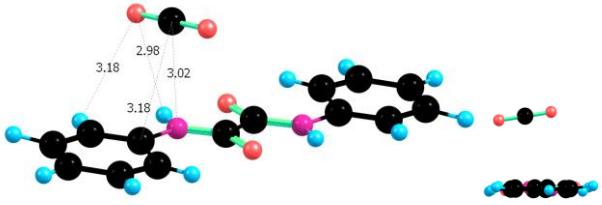	-10.25

G	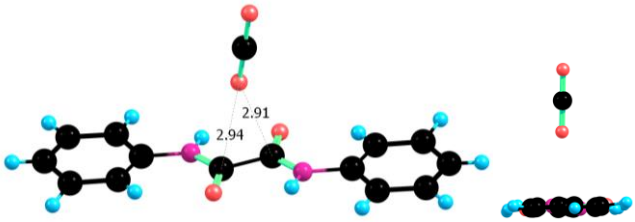	-7.61

Table 3: The structural details of the optimised configurations of $C_{14}H_{12}N_2O_2$ - CO_2 complexes corresponding to the strongest binding energies as predicted by the MP2/cc-pvqz level of theory.

Complex	Type of interaction	Distance, Å	Angle, degree	O=C=O angle, degree
A	H-Bond N-H···O(CO_2)	2.30 H···O(CO_2)	164.59 N-H···O(CO_2)	177.80
	Weak H-Bond C-H···O(CO_2)	2.67 H···O(CO_2)	142.93 C-H···O(CO_2)	
	 CO···C(CO_2)	2.78 O···C(CO_2)	150.00 C-O··· O(CO_2)	
B	H-Bond N-H···O(CO_2)	3.05 NH···O(CO_2)	175.29 N-H···O(CO_2)	177.88
	Weak H-Bond C-H···O(CO_2)	2.74 H···O(CO_2)	164.87 C-H···O(CO_2)	
	 C-O···C(CO_2)	2.74 O···C(CO_2)	173.79 C-O··· O(CO_2)	
C	H-Bond N-H···O_1(CO_2)	2.46 H···O_1(CO_2)	129.69 N-H···O_1(CO_2)	178.59
	H-Bond N-H···O_2(CO_2)	3.49 H···O_2(CO_2)	102.26 N-H···O_2(CO_2)	
	Weak H-Bond C-H···O_1(CO_2)	2.82 H···O_1(CO_2)	125.42 C-H···O_1(CO_2)	
	 C-O···C(CO_2)	2.91 O···C(CO_2)	106.17 C-O···O(CO_2)	
D	 C-H···O(CO_2)	2.8 H···O(CO_2)	44.7 C-H···O(CO_2)	178.82
	 C-O···C(CO_2)	2.97 CO···C(CO_2)	74.01 C-O···C(CO_2)	
E	 C-O···C(CO_2)	2.93 O···C(CO_2)	92.17 CO···C(CO_2)	178.56
	 O-C···O(CO_2)	2.90 C···O(CO_2)	86.93 OC···O(CO_2)	
F	 C-N··· C(CO_2)	3.02 N··· C(CO_2)	98.82 C-N··· C(CO_2)	179.75
	 N-H···O(CO_2)	2.98 H···O_CO_2	98.32 N-H···O_CO_2	
G	 O-C_1···O(CO_2)	2.94 C_1···O(CO_2)	95.57 O-C_1···O(CO_2)	179.87
	 O-C_2···O(CO_2)	2.91 C_2···O(CO_2)	97.98 O-C_2···O(CO_2)	

Table 4: The optimised MP2/cc-pvqz geometries and binding energies of C_6H_6- CO_2 complexes.

	Optimised Geometry	Binding Energy, kJ/mol
H	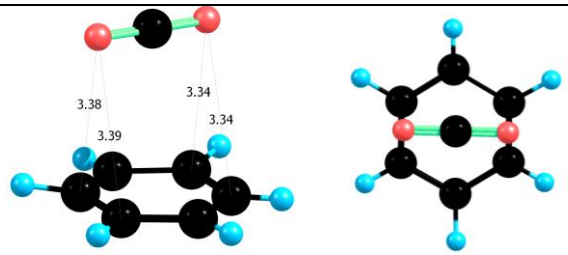	-11.13
I	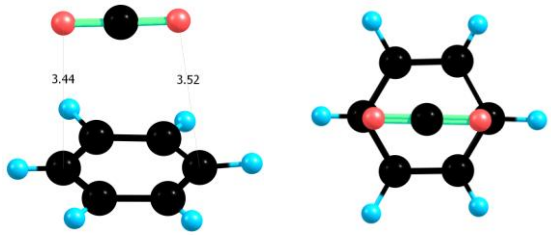	-10.93
J	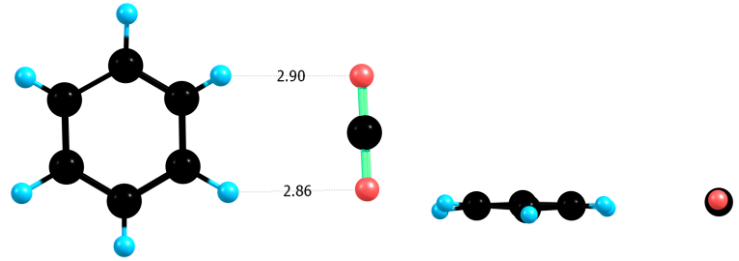	-3.83
K	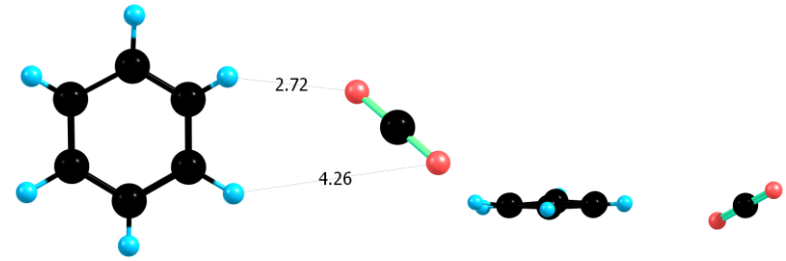	-3.06
L	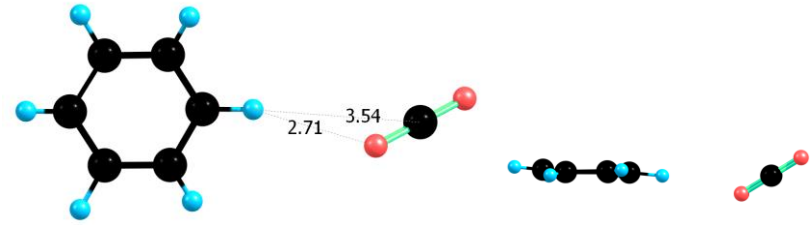	-2.42

Supporting Information

Analysis of High and Selective Uptake of CO_2 in an Oxamide-containing $\{Cu_2(OOCR)_4\}$ Based Metal Organic Framework

Nada H. Alsmail, Mikhail Suyetin, Yong Yan, Rafel Cabot, Cristina P. Krap, Jian Lü, Timothy L. Easun, Elena Bichoutskaia, William Lewis, Alexander J. Blake and Martin Schröder*

School of Chemistry, University of Nottingham, University Park, Nottingham NG7 2RD, UK

1. Spectroscopy

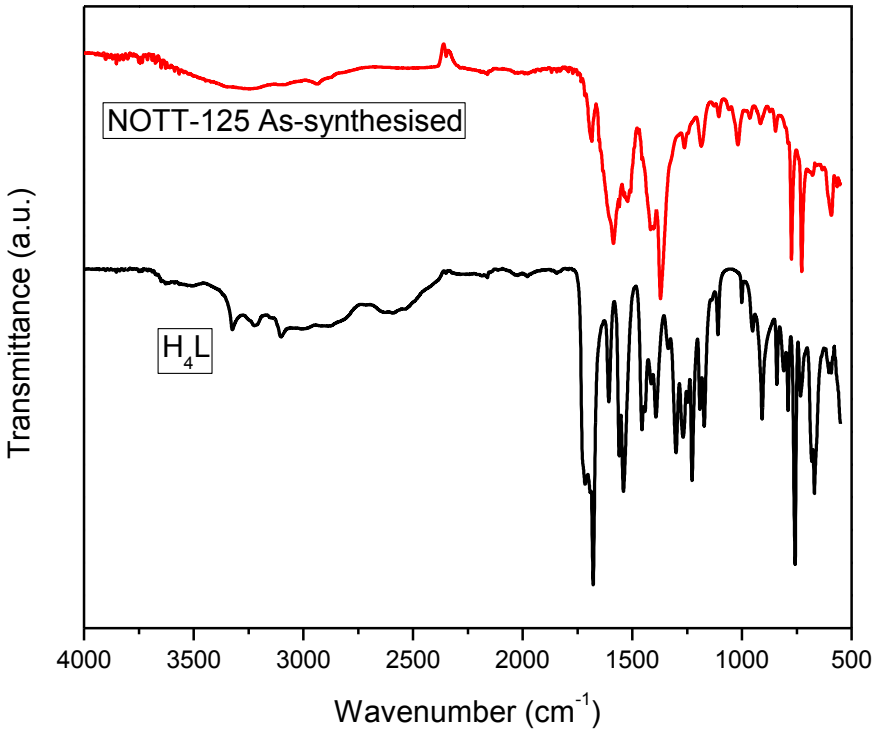

Figure S1. ATR-IR spectra of H_4L and of as-synthesised NOTT-125.

2. Single Crystal X-ray Structure Determination on NOTT-125

Single crystal diffraction data were collected on Oxford SuperNova CCD, Nottingham, UK. Details of the data collection are included in the CIF. The structure was solved by direct methods and developed by difference Fourier techniques, both using the SHELXTL software package.[1] The hydrogen atoms of the ligands were placed geometrically and refined using a riding model, and the hydrogen atoms of the coordinated water molecules could not be located but are included in the formula. The unit cell volume includes a large region of disordered solvent which could not be modelled as discrete atomic sites. We therefore employed PLATON/SQUEEZE[2] to calculate the contribution of the solvent region to the diffraction and thereby produced a set of solvent-free diffraction intensities.

Table S1. Crystal data and structure refinement details for NOTT-125

Identification code	NOTT-125
Empirical formula	C26 H38 Cu2 N4 O18
Formula weight	821.68
Temperature	120.01(10) K
Wavelength	1.54184 A
Crystal system, space group	Monoclinic, P 1 21/c 1
Unit cell dimensions	a = 27.9161(6) A alpha = 90 deg. b = 18.6627(4) A beta = 112.655(3) deg. c = 32.3643(8) A gamma = 90 deg.
Volume	15560.4(6) A^3
Z, Calculated density	12, 1.052 Mg/m^3
Absorption coefficient	1.501 mm^{-1}
F(000)	5088
Crystal size	0.1212 x 0.1047 x 0.0902 mm
Theta range for data collection	3.56 to 60.00 deg
Limiting indices	-31<=h<=23,-20<=k<=20,-36<=l<=36
Reflections collected / unique	91238 / 23087 [R(int) = 0.0519]
Completeness to theta = 60.00	99.9 %
Absorption correction	Gaussian
Max. and min. transmission	0.867 and 0.779
Refinement method	Full-matrix least-squares on F^2
Data / restraints / parameters	23087 / 0 / 919
Goodness-of-fit on F^2	1.013
Final R indices [I>2sigma(I)]	R1 = 0.0772, wR2 = 0.2127
R indices (all data)	R1 = 0.0916, wR2 = 0.2219
Largest diff. peak and hole	2.608 and -1.465 $e.Å^{-3}$

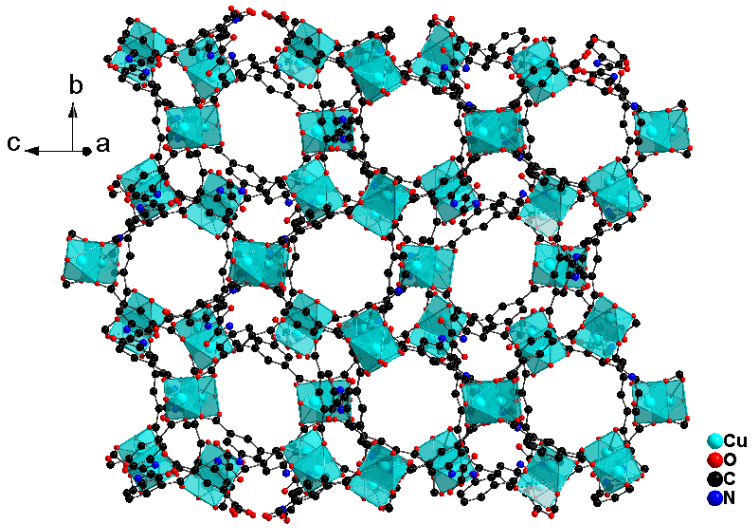

Figure S2. View of structure of NOTT-125.

3. TGA analysis

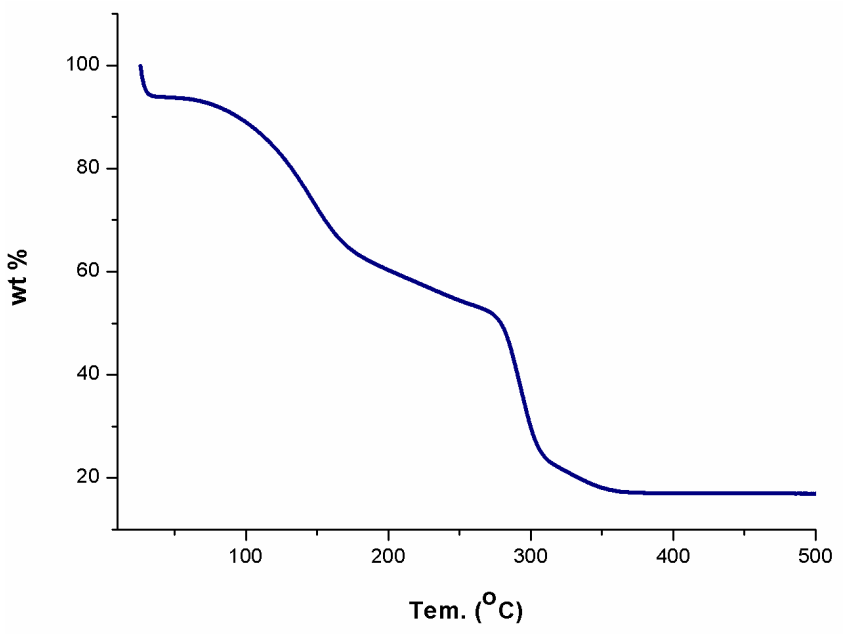

Figure S3. TGA plot of as-synthesised NOTT-125.

4. PXRD patterns

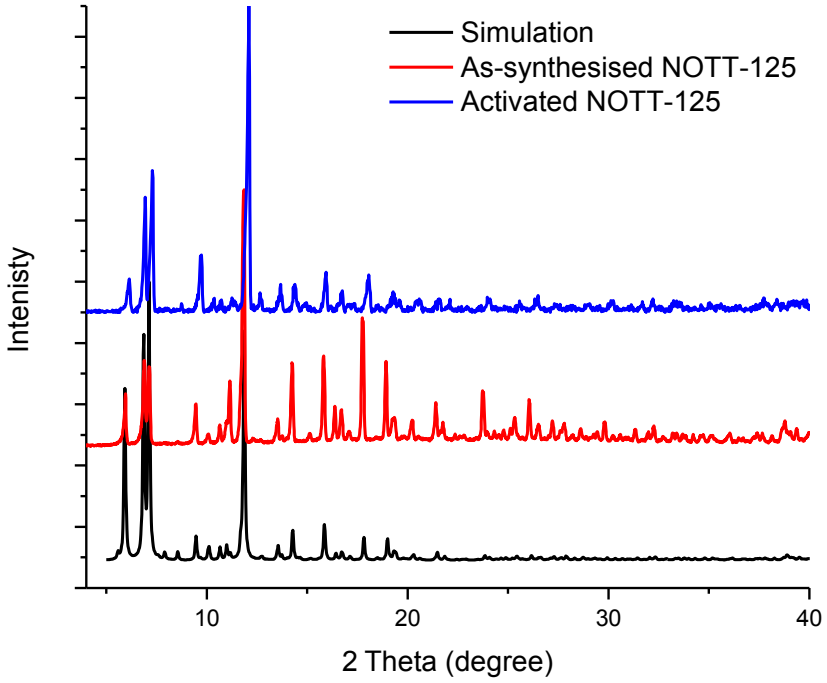

Figure S4. The PXRD patterns for NOTT-125. The activated sample was obtained by heating the acetone-exchanged sample at 100 ^{o}C under dynamic vacuum for 12 h.

5. BET surface area and pore size distribution

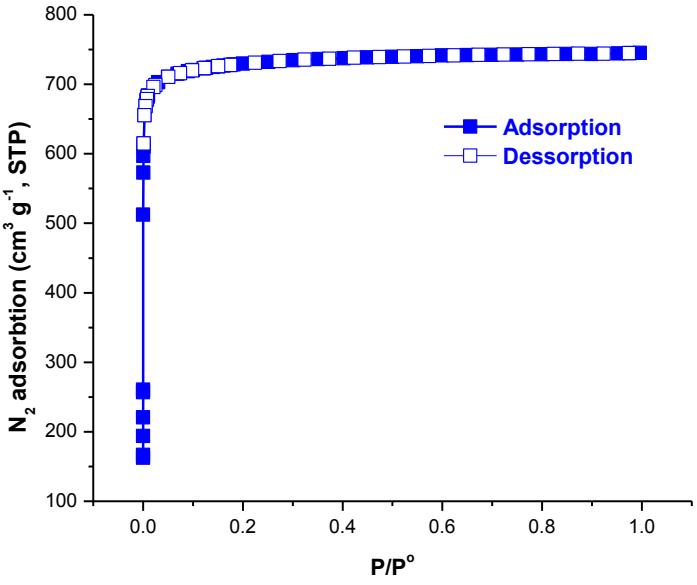

Figure S5. N_2 adsorption-desorption isotherms for NOTT-125a at 77 K.

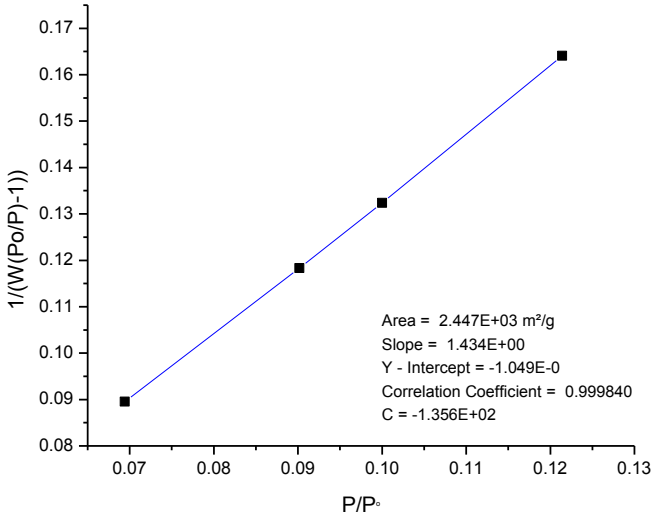

Figure S6. The BET plot derived from N_2 uptake in NOTT-125a in the range (P/P_0 = 0.07 – 0.13).

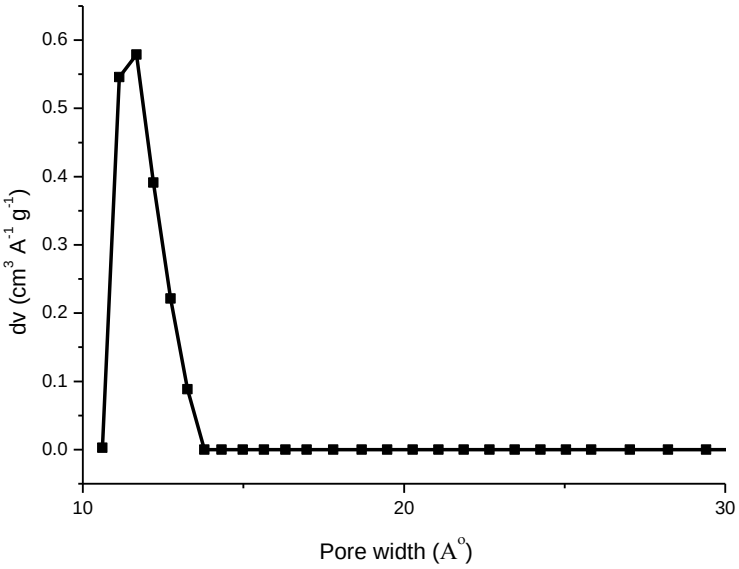

Figure S7. Pore size distribution for NOTT-125a calculated by NLDFT.

6. Heats of adsorption for CO_2 in NOTT-125

The CO_2 adsorption isotherms at 273 and 298 K were fitted to the virial equation (eq 3, virial method I):[3]

$$\ln\left(\frac{n}{P}\right) = A_0 + A_1 n + A_2 n^2 + A_3 n^3 + \ldots \quad (1)$$

where P is the pressure, n is total amount adsorbed and A_0, A_1, A_2 etc. are virial coefficients. The Henry's Law constant is given by $K_H = \exp(A_0)$. The enthalpy of adsorption at zero coverage was determined from the relationship:

$$\delta A_0 = R Q_{st}^{n=0} \delta(T^{-1}) \quad (2)$$

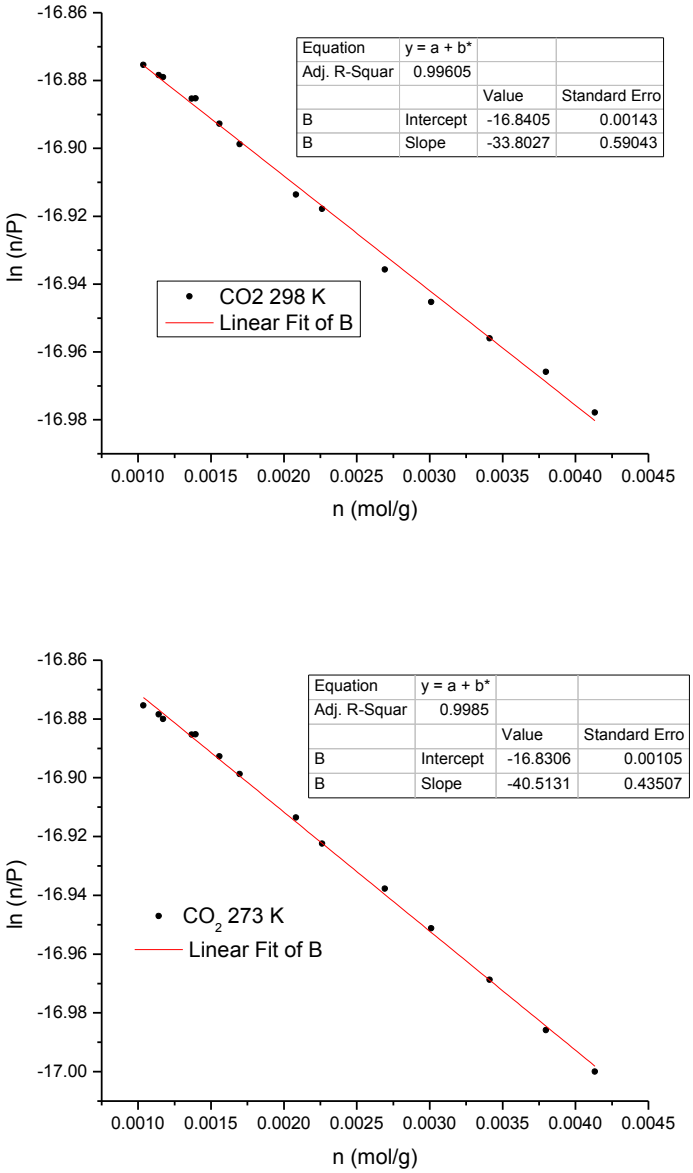

Figure S8. Virial analysis of the CO_2 isotherms for NOTT-125a at 298 and 273 K.

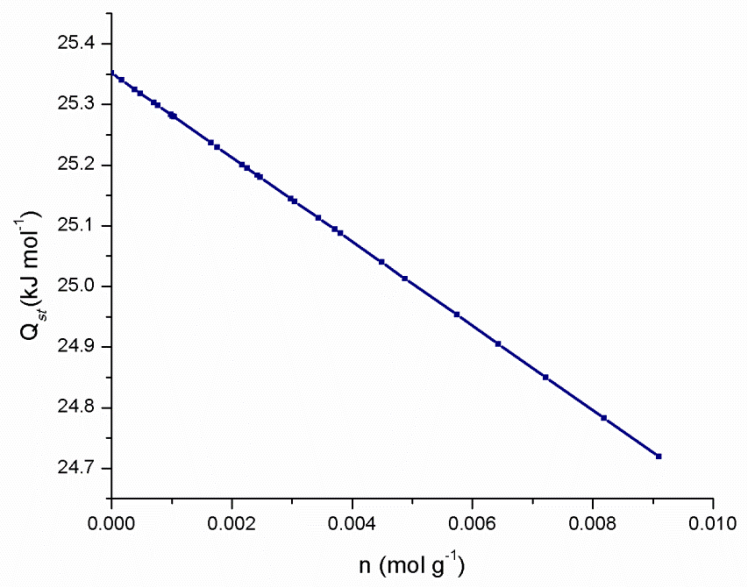

Figure S9. Heat of adsorption of CO_2 in NOTT-125a.

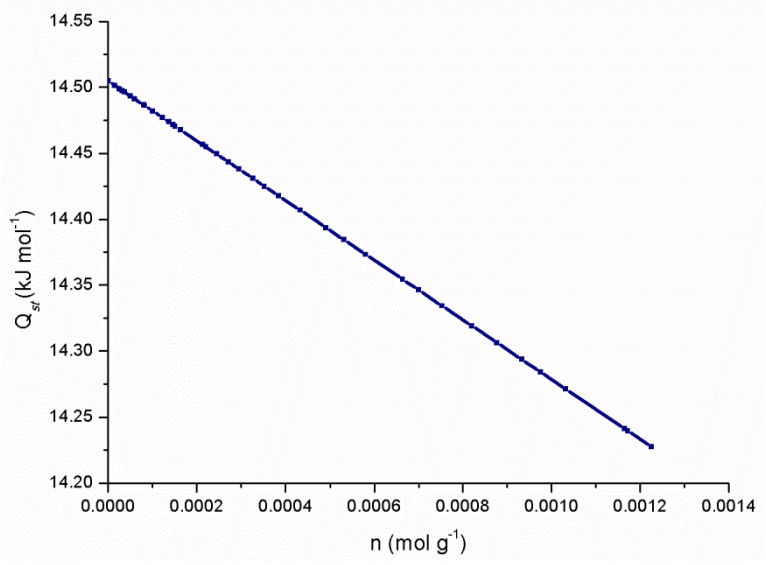

Figure S10. Heat of adsorption of CH_4 in NOTT-125a.

7. CO_2/N_2 and CO_2/CH_4 Selectivities in NOTT-125a

The Henry's Law selectivity for gas component *i* over *j* at a specific temperature was calculated based on Eq. 3

$$S_{ij} = K_{Hi}/K_{Hj} \quad (3)$$

The Henry's Law constants for N_2 and CH_4 adsorption at 298 and 273 K were calculated directly from the adsorption isotherms.

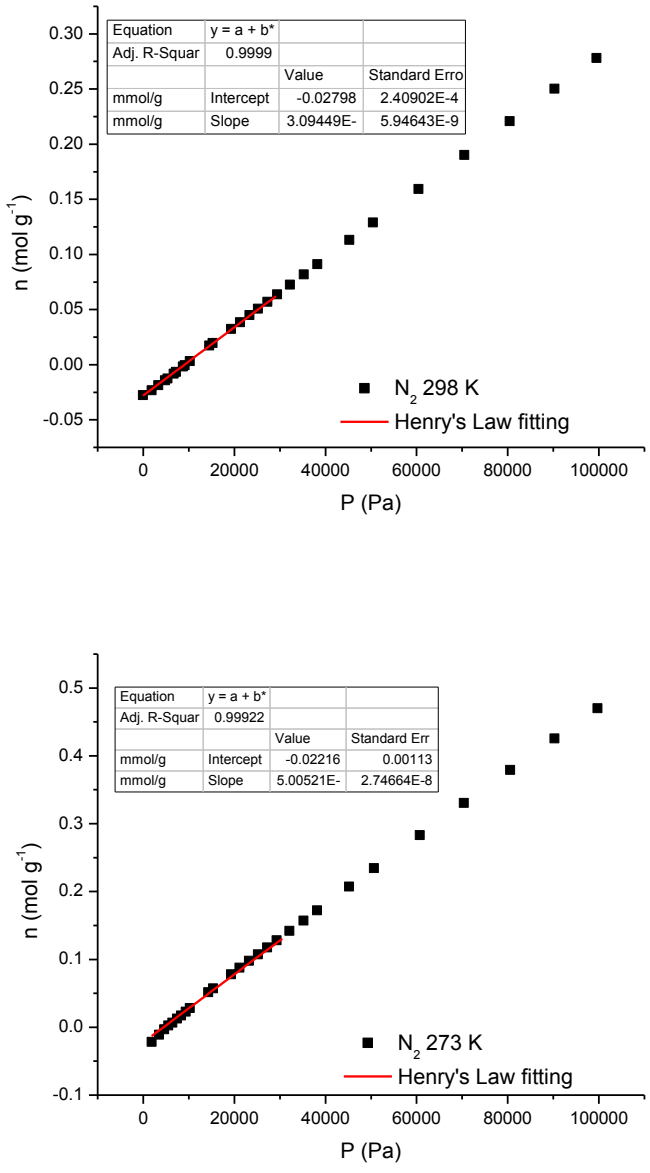

Figure S11. Fitting of the initial slope in N_2 isotherms for NOTT-125a collected at 273 and 298 K.

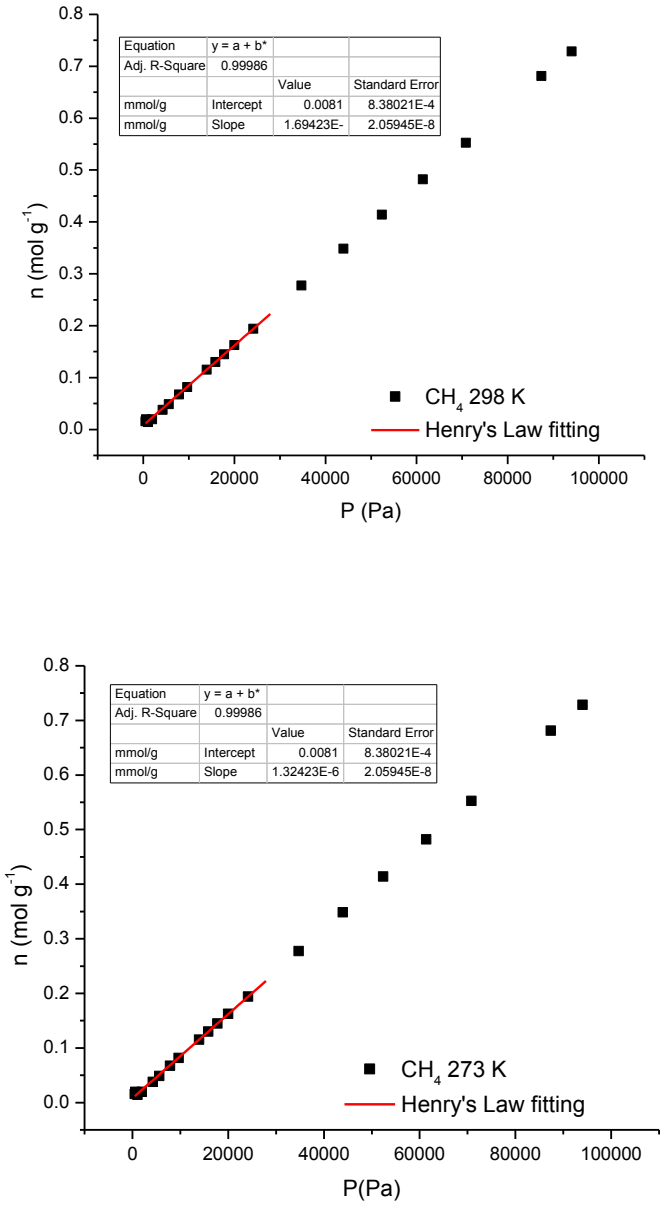

Figure S12. Fitting of the initial slope in CH_4 isotherms for NOTT-125a collected at 273 and 298 K.

8. H_2 sorption isotherms and heats of H_2 adsorption for NOTT-125a

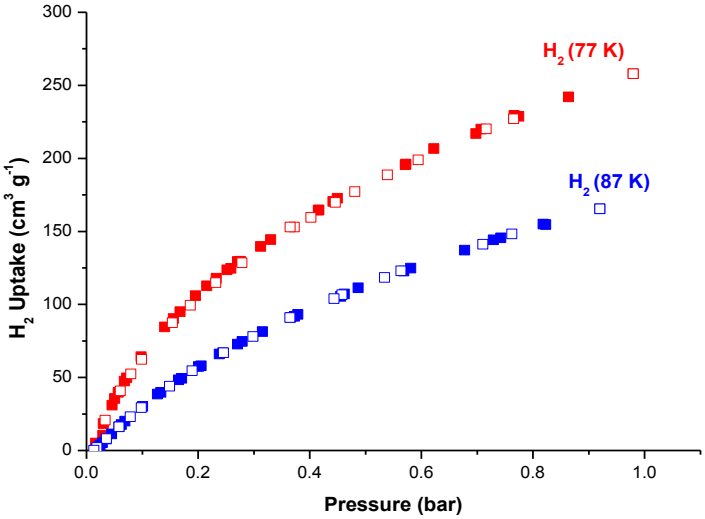

Figure S13. H_2 sorption isotherms for NOTT-125a at 77 and 87 K. wt% = 100(weight of adsorbed H_2/weight of host material).

A virial-type expression[4] (eq4, virial method II) was used to fit the combined isotherm data at 77 and 87 K:

$$\ln(P) = \ln(N) + (1/T)\sum_{i=0}^{m} a_i N^i + \sum_{j=0}^{n} b_j N^j \qquad (4)$$

Here, P is the pressure expressed in mbar, N is the amount adsorbed in mol/g, T is the temperature in K, a_i and b_j are Virial coefficients (temperature independent empirical parameters), and m and n represent the number of coefficients. The equation was fitted using the **R** statistical software package.[5] The values of the virial coefficients a_0 through a_m were then used to calculate the isosteric heat of adsorption using the following equation:

$$Q_{st} = -R\sum_{i=0}^{m} a_i N^i \qquad (5)$$

Here, Q_{st} is the coverage-dependent isosteric heat of adsorption and R is the universal gas constant.

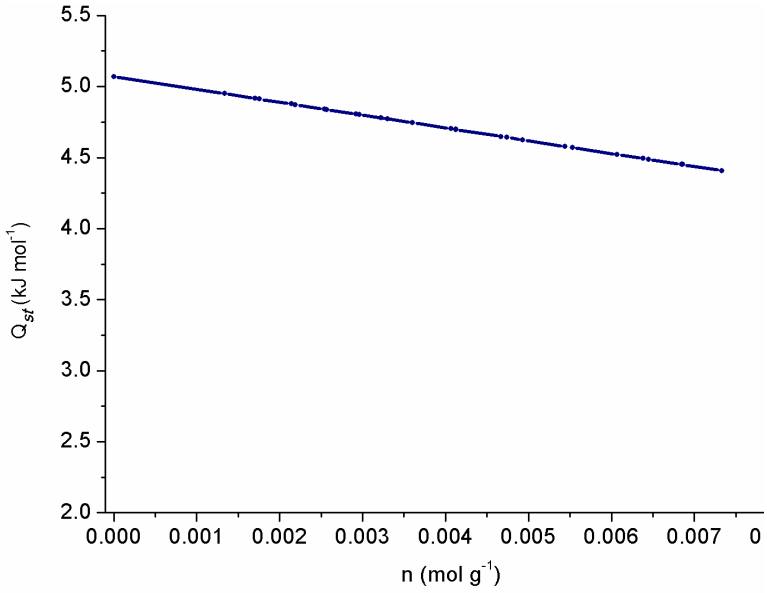

Figure S14. Heats of adsorption for H_2 in NOTT-125a.

9. Grand Canonical Monte Carlo simulations

Grand Canonical Monte Carlo (GCMC) calculations, as implemented in the MUSIC simulation suite,[6] were performed to calculate the adsorption of both CO_2 and CH_4 in NOTT-125a. In simulations of the CO_2 uptake the equilibration period of $2\cdot10^7$ steps was followed by $2\cdot10^7$ steps of production run; in the modelling of CH_4 uptake these values were taken to be $1.25\cdot10^7$ steps for equilibration period and $1.25\cdot10^7$ steps for the production run. Periodic boundary conditions have been applied to a modelling unit cell. The simulation parameters for CO_2 and CH_4 guest molecules were taken from the TraPPE force field.[7] For CO_2 molecules, the C−O bond length was taken to be 1.16 Å, and three charged Lennard-Jones interaction sites were employed with the following parameters: σ_O=3.05 Å, ε_O/k_B = 79 K for the oxygen atoms, and σ_C = 2.80 Å, ε_C/k_B = 27 K for the carbon atom. A point charge of +0.7 was placed at the centre of mass of the carbon atom and a point charge of −0.35 was placed at the oxygen atom. The CH_4 molecule was presented as united-atom with the following parameters: σ=3.73 Å, ε/k_B = 148.0 K. In the study of CO_2 capture, the structure of NOTT-125a was described

using the OPLS-AA force field.[8] For oxygen and copper atoms present in NOTT-125a the modelling atomic parameters were taken from reference 9 where they were adjusted for a correct description of the interaction between guest CO_2 molecules and the host MOF. The fugacity coefficients were calculated from the Peng-Robinson equation of state.[10] Both the framework and guest molecules were assumed to be rigid. The Lennard-Jones potential was used to describe the Van der Waals interactions with a cut-off distance of 15.0 Å. For CH_4 uptake, atom parameters of NOTT-125a structure were described by the DREIDING force field.[11] The partial charges on atoms of NOTT-125a were computed using the CHELPG approach and the B3LYP/6-31G* level of density functional theory, as implemented in the Q-Chem quantum chemistry package.[12]

References:

1. G. M. Sheldrick, *SHELXS*97. *Acta Crystallogr*., *Sect. A* 2008, **64**, 112–122.
2. A. L. Spek, *Acta Crystallogr*., *Sect. D*, 2009, **65**, 148–155.
3. I. P. O'Koye, M. Benham, K. M. Thomas, *Langmuir* 1997, **13**, 4054–4059.
4. J. Jagiello, T. J. Bandosz, J. A. Schwarz, *Langmuir* 1996, **12**, 2837–2842.
5. Download, instructions, and further details on the use and capabilities of this software package are available online at http://www.r-project.org.
6. A. Gupta, S. Chempath, M. J. Sanborn, L. A. Clark, R. Q. Snurr, *Mol. Simul.* 2003, **29**, 29–46.
7. J. J. Potoff, J. I. Siepmann, *AIChE Journal* , 2002, **47**, 1676−1682.
8. W. L. Jorgensen, D. S. Maxwell and J. Tirado-Rives, *J Am. Chem. Soc*. 1996, **118**, 11225-11236
9. Q. Yang and C. Zhong, *J. Phys. Chem. B*, 2006, **110**, 2, 17776–17783.
10. D.-Y. Peng, D. B. Robinson, *Ind. Eng. Chem. Fundamen*. 1976, **15**, 59–64.
11. S. L. Mayo, B. D. Olafson, W. A. Goddard III, *J. Phys. Chem*. 1990, **94**, 8897−8909.
12. Y. Shao *et al.*, *Phys. Chem Chem. Phys.* 2006, **8**, 3172–3191.